
Dilated Convolutions with Lateral Inhibitions for Semantic Image Segmentation

Yujiang Wang¹ Mingzhi Dong² Jie Shen^{1,†} Yiming Lin¹ Maja Pantic^{1,3}

¹Imperial College London ²University College London ³Facebook AI

yujiang.wang14@imperial.ac.uk mingzhi.dong.13@ucl.ac.uk

{jie.shen07, yiming.lin15, m.pantic}@imperial.ac.uk

Abstract

Dilated convolutions are widely used in deep semantic segmentation models as they can enlarge the filters' receptive field without adding additional weights nor sacrificing spatial resolution. However, as dilated convolutional filters do not possess positional knowledge about the pixels on semantically meaningful contours, they could lead to ambiguous predictions on object boundaries. In addition, although dilating the filter can expand its receptive field, the total number of sampled pixels remains unchanged, which usually comprises a small fraction of the receptive field's total area. Inspired by the Lateral Inhibition (LI) mechanisms in human visual systems, we propose the dilated convolution with lateral inhibitions (LI-Convs) to overcome these limitations. Introducing LI mechanisms improves the convolutional filter's sensitivity to semantic object boundaries. Moreover, since LI-Convs also implicitly take the pixels from the laterally inhibited zones into consideration, they can also extract features at a denser scale. By integrating LI-Convs into the Deeplabv3+ architecture, we propose the Lateral Inhibited Atrous Spatial Pyramid Pooling (LI-ASPP) and the Lateral Inhibited MobileNet-V2 (LI-MNV2). Experimental results on three benchmark datasets (PASCAL VOC 2012, CelebAMask-HQ and ADE20K) show that our LI-based segmentation models outperform the baseline on all of them, thus verify the effectiveness and generality of the proposed LI-Convs.

1 Introduction

Since the introduction of the pioneering Fully Convolutional Networks (FCN) [27], deep Convolutional Neural Networks (CNNs) [9, 55, 26, 54, 20] have made impressive progress in semantic image segmentation, a task that performs per-pixel classifications. In deep CNN models, a series of convolutions and spatial poolings are applied to obtain progressively more abstract and more representative feature descriptors with decreasing resolutions. As a consequence, the deepest features can have significantly lower resolution than the original image (e.g. only 1/16 or 1/32 of the input size in FCN [27]), hence it would be difficult to decode these features into the segmentation map at the same size of the input image without losing details. This is a crucial challenge in the semantic segmentation task.

Dilated convolutions [19], which are first applied to the semantic segmentation task by [52, 6], can effectively overcome such difficulties and thus are widely employed in state-of-the-art segmentation methods [26, 9, 51, 5, 46]. By inserting zeros (*dilation*) into the convolutional filters, dilated convolutions can observe features from larger areas without increasing the kernel parameters, which is important to the extractions of global semantic features. Besides, it can also produce feature maps

[†]Corresponding author.

that are invariant input resolutions. In practice, dilated convolutions can be utilised to retain the resolution of the feature maps when encoding representations in the backbone network [53, 46], typically by replacing certain convolutional layers with dilated ones. It can also be employed during the decoding stage to generate more robust semantic labels, e.g. the Atrous Spatial Pyramid Pooling (ASPP) [8, 7] adopts three parallel dilated convolutions with different dilation rates to aggregate the multi-scale contextual information.

Despite its broad applications, dilated convolutions still have several limitations. The pixels around semantically meaningful contours separate different objects and possess stronger semantic information. In dilated convolution, however, the importance of those pixels are not explicitly accentuated, and therefore such positional significance has to be implicitly learnt. This can lead to ambiguous and misleading boundary labels. Various approaches have been proposed to compensate for such problems and to refine the contour predictions, including the Conditional Random Fields (CRF) [7, 4] and the decoder component in Deeplabv3+ [9]. However, dilated convolution’s sensitivity on spotting semantically meaningful edges still leaves room for improvement.

Additionally, although the receptive field of dilated filters is enlarged, the total number of sampled pixels stay the same, which only consist of a small fraction of pixels in the area. The sparse sampling can somehow impair the potentials for dense prediction tasks like semantic segmentation. Similar concerns were address in [41, 46, 11, 50], and the proposed improvements include a denser Gaussian sampling process [41], a hybrid dilated convolution module [46] and the deformable convolutional filters [11].

In this paper, we propose to overcome the drawbacks in dilated convolutions from a biologically-inspired perspective, which is to leverage the Lateral Inhibition (LI) mechanism in the human visual system. Lateral inhibition [17, 36, 45] is a neurobiological phenomenon that a neuron’s excitation to a stimulus can be suppressed by the activation of its surrounding neurons. Because of the LI mechanism, our retina cells are sensitive to the spatially varying stimulus such as the semantic borderlines between objects, which is crucial to the inborn segmentation abilities of our eyes. See Fig. 1 (*Left*) for an intuitive illustration of the LI mechanism.

Motivated by such observations, we propose a dilated convolution with lateral inhibitions (LI-Convs) to enhance the convolutional filter’s sensitivity to semantic contours. The LI-Convs also sample the receptive window in a denser fashion by implicitly making inferences on pixels within the lateral inhibited zones. To evaluate LI-Convs, we follow the Deeplabv3+ [9] segmentation models and present two LI-based variants which are 1. the Lateral Inhibited Atrous Spatial Pyramid Pooling (LI-ASPP) for decoding semantic features, and 2. the Lateral Inhibited MobileNet-V2 (LI-MNV2) as the backbone network for encoding features. The performance of LI-ASPP and LI-MNV2 surpass the baseline on three segmentation benchmark dataset: PASCAL VOC 2012 [12], CelebAMask-HQ [23] and ADE20K [56], which verifies the effectiveness and generality of the proposed LI-Convs.

2 Related Works

Semantic Image Segmentation Fully Convolutional Networks (FCN) [27] is the pioneering work of using deep models for semantic segmentation. The fully connected layers in deep image classification models are replaced with convolutional ones to produce semantic heat maps for segmentation predictions. The resolution of such heat maps is typically much smaller than that of the input image (e.g. $1/32$), and various works are proposed to compensate the information loss during decoding such features, including the de-convolutional layers [33, 37, 34], the skip-connections of low-level features [2, 16] and dilated convolutions [52, 8, 51, 26, 5]. Yu *et al.* [52] stacks dilated convolutional layers with different dilation rates in a cascaded manner, leading to a context module for aggregating the multi-scale contextual information. Deeplabv3 [8] builds an Atrous Spatial Pyramid Pooling (ASPP) module consisting of three parallel dilated convolutions, one 1×1 convolution and one image-level pooling, and it also employs dilated convolutions in the backbone network. DenseASPP [51] introduces dense connection into the ASPP module, while the technique of Neural Architecture Search [58] is utilised by [5] to search for an optimal decoding structure of organising dilated convolutions layers. For other segmentation practice [35, 47, 28, 48], readers are referred to [31] for more details.

Dilated Convolutions Dilated convolutions, also known as atrous convolutions, is first introduced by Holschneider *et al.* [19] in signal analysis and have broad applications such as object detection [24, 32], lip-reading [49, 30] and optical flow [57, 44]. It is first applied to semantic segmentation

by authors of [52, 6] to enlarge filter’s receptive fields without sacrificing the spatial resolution. Conditional Random Fields (CRF) are involved in [4, 7] as a post-processing procedure to refine the ambiguous semantic contour predictions. Similar ideas can be found in Deeplabv3+ [9], which designs a decoding module to incorporate low-level backbone features to improve the qualities of contouring pixels. Deformable convolutions [11] introduce the *offsets* into the sampling grids of filters to better model the spatial relationships. Gaussian kernels are adopted by [41] to obtain pixels at a wider range in dilated convolutions. Wang *et al.* [46] observe the *gridding* effects brought by the fixed sampling locations in dilated kernels and demonstrate a hybrid dilated convolution with different dilated rates. Different from those approaches, we employ the lateral inhibition (LI) mechanisms [17] to enhance the dilated convolutions’ sensitivity on semantically meaningful contours and to implicitly sample features in a denser fashion.

Lateral Inhibitions The study on the eyes of horseshoe crab (*Limulus*) performed by Hartline *et al.* [17] reveals the lateral inhibition (LI) effects in visual systems, where the excitation of neighbouring neurons can suppress a cell’s response to the stimuli. Although lateral inhibitions are mainly studied in the field of neuroscience [38, 43, 36], the computer vision community has also shown interests in this mechanism. The recurrent neural network with lateral inhibitions is studied in [29] and it is shown that LI can improve the robustness and efficiency of the network. Authors of [13] introduce LI into a shallow CNN to improve image classification. Similar ideas can be found in the work for colour video segmentation [14]. Those network architectures are somehow too shallow to be useful for recent methods using deep backbones like MobileNet-V2 (MNv2) [40] or ResNet [18]. Recently, authors of [3] employ LI in VGG model [42] to improve the performance on saliency detection. However, none of the previous works has evaluated LI’s potentials for semantic segmentation, while their methods of integrating LI do not touch the core mechanisms in deep CNNs such as the convolutional operations. In this work, however, lateral inhibitions work closely with the convolutional filters to fundamentally augment the model’s segmentation powers.

3 Dilated Convolutions with Lateral Inhibitions

3.1 Definition

Define $\Psi_k = \mathbb{Z}^2 \cap [-k, k]^2$ where $k \in \mathbb{Z}_{\geq 0}$, and let a discrete function $F : \Psi_k \mapsto \mathbb{R}$ represents a convolutional filter of size $(2k + 1)^2$. Define another discrete function $G : \mathbb{Z}^2 \mapsto \mathbb{R}$ representing features of arbitrary sizes. Let d be the dilation rate, a dilated convolutional operator $*_d$ is written as

$$(F *_d G)(\mathbf{p}) = \sum_{d\mathbf{m}+\mathbf{n}=\mathbf{p}} F(\mathbf{m})G(\mathbf{n}) \quad (1)$$

where $\mathbf{p}, \mathbf{m}, \mathbf{n} \in \mathbb{Z}^2$. Note that $*_d$ turns into a regular convolutional operator when $d = 1$, i.e. no dilation is inserted.

With the introduction of lateral inhibitions (LI), the activation of each sampled pixel, i.e. $G(\mathbf{n})$ in Eq. 1, would be suppressed by its neighbours within a certain range. Let the lateral inhibitions come from a square region of size $(2t + 1)^2$ centred on \mathbf{n} where $t \in \mathbb{Z}_{\geq 0}$, and refer this region as the lateral inhibition zone (the LI zone). Define $\Psi_t = \mathbb{Z}^2 \cap [-t, t]^2$ and let $L : \Psi_t, \mathbb{Z}^2 \mapsto \mathbb{R}$ be a discrete function describing the spatially-varying inhibition intensities in the LI zones, the amount of the total inhibitions received by a sampled pixel $G(\mathbf{n})$ can be described as $\sum_{\mathbf{u}+\mathbf{v}=\mathbf{n}} L(\mathbf{u}, \mathbf{n})G(\mathbf{v})$ where $\mathbf{u}, \mathbf{v} \in \mathbb{Z}^2$. Consequently, a dilated convolutional operator with lateral inhibition \star_d (LI-Conv) can be defined as:

$$(F \star_d G)(\mathbf{p}) = \sum_{d\mathbf{m}+\mathbf{n}=\mathbf{p}} F(\mathbf{m})(G(\mathbf{n}) - \sum_{\mathbf{u}+\mathbf{v}=\mathbf{n}} L(\mathbf{u}, \mathbf{n})G(\mathbf{v})). \quad (2)$$

Note that Eq. 2 is essentially an extension of Eq. 1 with the introduction of LI terms. Fig. 1 (*Middle, Right*) provides an intuitive comparison between dilated convolution and the proposed LI-Conv.

We can also "dilate" the lateral inhibition zone to efficiently expand its field-of-views, in similar way to that of dilated convolutions. Denote the dilation rate in LI zones as e , a generalised LI-Conv operator \star_d^e is denoted as

$$(F \star_d^e G)(\mathbf{p}) = \sum_{d\mathbf{m}+\mathbf{n}=\mathbf{p}} F(\mathbf{m})(G(\mathbf{n}) - \sum_{e\mathbf{u}+\mathbf{v}=\mathbf{n}} L(\mathbf{u}, \mathbf{n})G(\mathbf{v})). \quad (3)$$

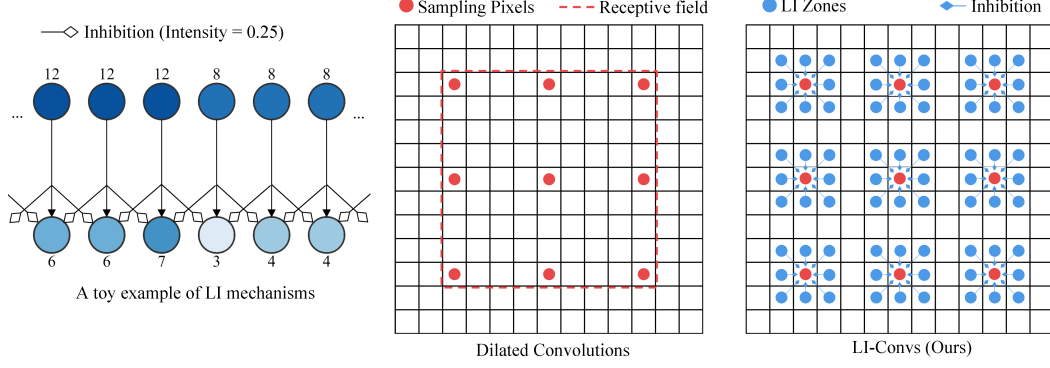


Figure 1: *Left*: A toy example to illustrate the lateral inhibition mechanisms where the LI intensity is set to 0.25. The difference between the two neurons at the centre (representing a semantic contour) becomes more significant after LI. *Middle*: A 3×3 convolutional filter where $d = 4$. The sampled pixels (denoted as red dots) only comprises a small fraction of all pixels in the receptive field. *Right*: An illustration of the proposed LI-Convs with 3×3 lateral inhibition zones. Each sampled pixel receives inhibition signals from eight neighbours to enhance sensitivity on semantic contours and to extract information at a denser scale.

Although a wide variety of kernel forms can be taken by the LI intensity descriptor L , we opt for an intuitive formulation that is also easy to implement. In particular, $L(\mathbf{u}, \mathbf{n})$ in Eq. 3 simply takes the production of a differentiable weight $W_L \in [0, 1] \cap \mathbb{R}$ and an exponentially decaying factor that is related to the distance between \mathbf{u} and \mathbf{n} , which can be described as

$$L(\mathbf{u}, \mathbf{n}) = W_L \exp\left(\frac{D^2(\mathbf{u}, \mathbf{n})}{2\sigma^2}\right) \quad (4)$$

where σ is a parameter representing the standard deviation and $D(\mathbf{u}, \mathbf{n})$ refers to a certain distance measurement between \mathbf{u} and \mathbf{n} . Here we employ the Euclidean distance.

3.2 Implementation of LI-Convs

We take a straight-forward approach to implement the LI-Convs in Eq. 3. We first design a Lateral Inhibition layer (the LI layer) to perform pixel-wise lateral inhibitions, while a dilated convolutional layer is subsequently applied to the inhibited features. The LI layer is essentially a light-weight module that can be flexibly inserted into deep models, while it can be easily implemented as a convolutional layer with specifically shaped filters. In particular, let a discrete function $K : \Psi_t \mapsto \mathbb{R}$ represent one such LI filter, K can be described as:

$$K(\mathbf{u}) = \begin{cases} 1.0 & \mathbf{u} = \mathbf{0}. \\ -W_L \exp\left(\frac{D^2(\mathbf{u}, \mathbf{0})}{2\sigma^2}\right) & \mathbf{u} \neq \mathbf{0}. \end{cases} \quad (5)$$

Note that the LI filter K has identical size with the LI zones which is $(2t + 1)^2$, and applying K with a stride of 1 can generate pixel-wise inhibited features. We empirically set σ in Eq. 5 to a fixed value during training, thus there is only one weight W_L to learn for each LI filter, which is significantly less than that of regular convolutional filters. In practice, we learn the lateral inhibition weights in a channel-wise manner, i.e. each LI filter learns a separate W_L . Therefore, a LI layer will introduce a total of C learnable weights where C is the channel number of the input tensor.

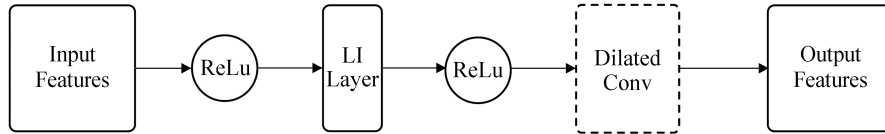


Figure 2: The structure of LI-Convs. The lateral inhibitions is first calculated by the LI layer, and the inhibited features are fed into the dilated convolution layer. The dilated convolution part can be any kind of convolution implementations such as the depthwise one [10].

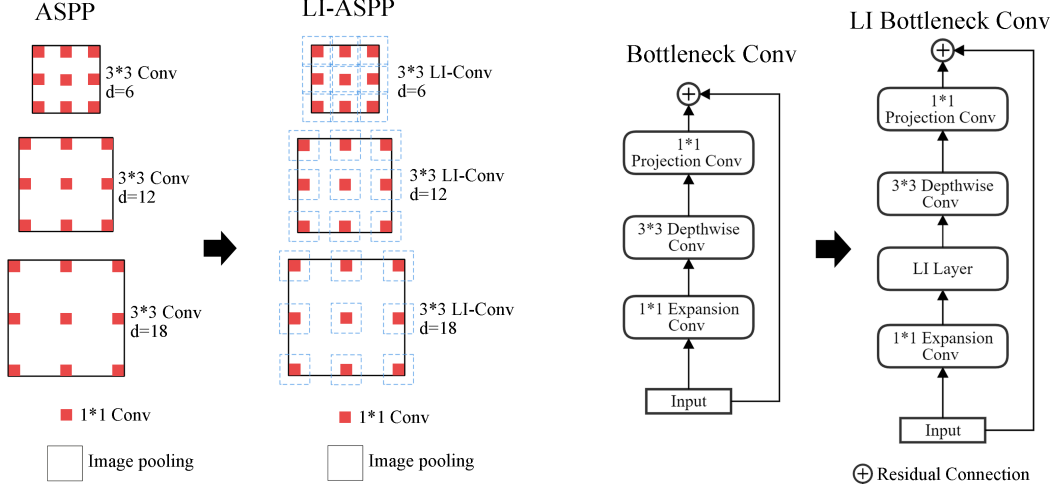


Figure 3: *Left:* The structures of ASPP and LI-ASPP. ASPP consists of five parallel branches including three dilated convolutions, which are replaced with the proposed LI-Convs in LI-ASPP. *Right:* The structures of the *residual bottleneck* convolution in MobileNet-V2 and the LI bottleneck. The LI layer is inserted between the 1×1 expansion convolution and 3×3 depthwise convolution.

A detailed illustration for the LI-Convs implementations can be found in Fig 2. A ReLU activation is first applied to remove negative activations. Then a LI layer with filters in Eq. 5 is employed to extract inhibited features, followed by another ReLU layer. This is then followed by a dilated convolution layer, which can take any form such as the depthwise conv [10].

3.3 LI-ASPP and LI-MNV2

We introduce the proposed LI-Convs into the state-of-the-art segmentation model Deeplabv3+ [9] to evaluate the proposed LI-Convs. As shown in Fig. 3 (*Left*), we have replaced the three 3×3 parallel dilated convolution operations in Atrous Spatial Pyramid Pooling (ASPP) [9] with the proposed LI-Convs, leading to the LI-ASPP model. Besides, we also investigate the potentials of LI layer in the backbone network such as the MobileNet-V2 (MNV2). In particular, we insert the LI layer into the *residual bottleneck* (RB) of MobileNet-V2 [40], between the 1×1 expansion convolution and 3×3 depthwise convolution, as illustrated in Fig. 3 (*Right*). We refer to this structure as the LI bottleneck layer. In the original MNV2 architecture, there is a total of 17 *residual bottleneck* layers, and we replace the 10th, 13th and 16th (16th refers to the second-highest RB layer) *residual bottlenecks* with the LI bottlenecks to obtain the LI-MNV2 network.

4 Experiments

4.1 Datasets

We conduct our experiments on three public benchmark segmentation datasets, which are PASCAL VOC 2012 [12], CelebAMask-HQ [23] and ADE20K [56]. There are a total of 21 semantic classes in PASCAL VOC 2012 dataset [12] which contains 1,464/1,449/1,456 pixel-wise annotated images for train/validation/test. Following [15, 9], we use an augmented train set with a total of 10,582 annotated images. CelebAMask-HQ [23] is a large-scale face parsing dataset with 30,000 pixel-wise labelled face images of 19 classes, and they are split into sets with 24,183/2,993/2,824 images for train, validation and test. ADE20K [56] is a benchmark dataset for scene parsing with 20,210/2,000/3,000 pixel-wise labelled images for train/validation/test. It is a quite challenging dataset, as there are a total of 151 classes in this dataset, and the huge variations of image resolutions also increase the difficulties. We utilise the validation set to evaluate performance on PASCAL VOC 2012 and ADE20K datasets, considering that their test sets are not publicly available, while we follow the standard protocol on CelebAMask-HQ dataset and use the test set for evaluation.

Table 1: The performance of different LI-Conv’s parameters on Pascal Voc 2012 validation set for LI-ASPP and LI-MNV2, respectively. "RB" refers to the *Residual Bottleneck* in MNV2 [40].

Backbone	Decoding model	Positions of LI-Convs	LI Zone Sizes	LI Rates e	W_L Init. Range	mIoU (%)
MNV2	LI-ASPP	Three dilated convolution layers in ASPP with rates {6, 12, 18}	3 * 3	1	[0.0, 0.0]	72.49
			3 * 3	{1,3,5}	[0.0, 0.0]	72.56
			3 * 3	5	[0.05, 0.15]	72.43
			5 * 5	1	[0.05, 0.15]	72.13
			3 * 3	1	[0.05, 0.35]	72.64
			3 * 3	1	[0.0, 0.15]	72.93
LI-MNV2	ASPP	{1 – 6} th RB	3 * 3	1	[0.0, 0.0]	72.07
		16 th RB				72.21
		{3, 6, 10, 13, 16} th RB				71.78
		{13, 16} th RB				72.43
		{10, 13, 16} th RB				72.5

4.2 Experimental Setup

Evaluation metric Mean Intersection-over-Union (mIoU) is the most widely used evaluation metric for the segmentation task, and we adopt it to evaluate the quality of model predictions. We also report the model parameters and the FLOPs to provide more comprehensive analyses.

Training Settings We generally follow the training settings in Deeplabv3+ [9], while we have also made some modifications to suit our needs. Particularly, we use the ImageNet [39] checkpoint provided by MobileNet-V2 authors [40] to initialise LI-MNV2, while the weights of LI-ASPP are randomly initialised. Note that we do not use the MS COCO dataset [25] to pre-train the model. During training, we set the image crop size to be 513 * 513 for the PASCAL VOC 2012 and CelebAMask-HQ datasets and 257 * 257 for ADE20K dataset. We train for 120 epochs using a batch size of 16 and the SGD method [22] is applied to optimise the pixel-wise cross-entropy loss with L2-regularisation. The initial learning rate is set to 0.01 with the decaying policy described in [9]. The *output stride*, which is defined in [8] denoting the ratio of original input resolution to the final feature’s resolution, is set to be 16 for all datasets. We adopt strategies in [9, 8] to use the BatchNorm layers [21] and to randomly scale the training data for augmentation. Depthwise convolution [10] is used in the ASPP implementations following [9]. During evaluations, we set the *output stride* to be 16 for all datasets, and we use a crop size of 257 * 257 for ADE20K and 513 * 513 for PASCAL VOC 2012 and CelebAMask-HQ.

LI Layer Settings A lateral inhibition layer has several key hyper-parameters that can affect the performance. We fine-tune those parameters on the Pascal Voc 2012 validation set to determine a best-performing combination. Particularly, for LI-ASPP, we set the size of LI zones to be 3 * 3, the value for the standard deviation σ in Eq. 5 is selected to be 1.0, the LI rate e in Eq. 3 is set to 1, and we uniformly initialise the LI intensity W_L in Eq. 5 between 0.0 and 0.15 during training. Almost identical LI settings are applied in LI-MNV2, except that all LI intensities W_L are initialised as 0.0 such that the training can start smoothly without breaking any existing organisations in ImageNet checkpoint. Moreover, we evaluate different positions of adding LI bottlenecks in the MNV2 architectures, and a general trend can be observed that adding LI to higher layers can produce better performance than to bottom ones.

Implementations We implement our method in the Tensorflow framework [1]. For the implementation of the baseline Deeplabv3+ [9] model, we directly use the code provided by authors. To ensure a fair comparison, the decoder module in Deeplabv3+ [9] is disabled for all experiments. It takes around one day per GPU (2080TI) to train a model (LI-MNV+LI-ASPP) on Pascal Voc 2012 dataset, and it requires about 2.5/0.6 days to do so on CelebAMask-HQ and ADE20K datasets.

Table 2: Performance of different methods on the Pascal Voc 2012 and ADE20K (validation set) and on the CelebAMask-HQ (test set). To provide a fair comparison, we repeat each experiment for three times to report the means and the standard deviations, and the model parameters and FLOPs (for crop size $513 * 513$) are also included.

Method	mIoU (%)			Parameters (Kilo)	FLOPs (Mega)
	Pascal Voc 2012	CelebAMask- HQ	ADE-20K		
MNV2+ASPP (Deeplabv3 [8])	71.85 \pm 0.30	74.69 \pm 0.31	30.02 \pm 0.11	2568.02	6479
MNV2 + LI-ASPP	72.63 \pm 0.24	75.25 \pm 0.05	30.43 \pm 0.27	2568.98	6498
LI-MNV2 + ASPP	72.47 \pm 0.34	75.29 \pm 0.15	30.44 \pm 0.36	2569.94	6517
LI-MNV2 + LI-ASPP	72.95\pm0.24	75.55\pm0.13	30.52\pm0.18	2570.52	6528

4.3 Results

In Table 1 we demonstrate the performance of different LI parameters on Pascal Voc 2012 validation set for LI-ASPP and LI-MNV2, respectively. In the LI-ASPP experiments, we investigate the performance of different settings of LI hyper-parameters such as the size of LI Zones, the LI rates e and the initialisation range for W_L . As shown in Table 1, using a $3 * 3$ LI zone and let $e = 1$ can generally yield better performance than other settings like a $5 * 5$ LI Zone or $e = 5$. LI-ASPP achieves the best performance when W_L is randomly initialised within $[0.0, 0.15]$, and therefore we opt for this setting for LI-ASPP.

In addition, we evaluate different options of adding LI-Convs in the *Residual Bottleneck* (RB) layers of the MNV2 architecture [40]. It can be spotted from Table 1 that adding LI mechanisms to the early RB layers (e.g. the earliest six RB layers) cannot promote the accuracy. In contrast, LI-Convs integrated with top layers such as the $\{10, 13, 16\}^{th}$ RB layers can produce higher mIoUs. This observation is somehow in line with the expectations since the higher-level layers are generally encoding more semantic representations, which can better benefit from the improved sensitivity to semantic contours introduced by LI layers.

In Table 2, we report the evaluation results of different methods on the three segmentation benchmark datasets, where each experiment is repeated for three times to present the mean and standard deviations (SD). Compared with the baseline method (MNV2+ASPP i.e. Deeplabv3 [8]), LI-MNV2 and LI-ASPP both demonstrate superior performance when used solely, while the best mIoUs on three datasets are all achieved by using them together. Particularly, our method (LI-MNV2+LI-ASPP) gains a relative improvement of 1.53%, 1.1% and 1.6% over the baseline on Pascal Voc 2012, CelebAMask-HQ and ADE-20K datasets, respectively, with more stabilised performance featured by smaller SDs. The model’s parameters and FLOPs, however, are slightly increased by 0.10% and 0.75%, which is arguably acceptable considering the accuracy compensations. Basing on those results, the effectiveness and generality of the proposed LI-Convs are therefore justified.

4.4 Discussion

How the LI layer works To intuitively understand the LI mechanisms, we dive into the channel-level features to visualise the patterns before and after LI layers. As demonstrated in Fig. 4, we plot several feature channels before and after the LI layers in LI-ASPP on CelebAMask-HQ dataset. It can be discovered that although the intensity of activation is suppressed globally after the LI layer, the inhibited feature exhibits more recognisable patterns with clarified and emphasised contours, which can be more desirable in the segmentation domain.

What interests the model In Fig. 5, we visualise the class-level heat maps and the segmentation predictions generated by the baseline (MNV2+ASPP) and our method (LI-MNV2+LI-ASPP) on CelebAMask-HQ. We utilise deeper reds to denote higher positive neurons responses (more model attention) in heat maps, and vice versa for deeper blues. Compared with the baseline, the semantically meaningful contouring areas receive more attention from our model, e.g. the "glasses" and "skin" heat maps in Fig. 5. Such kind of contour sensitivity can be reasonably attributed to the proposed



Figure 4: Visualisations of the channel-level features before and after LI layers on CelebAMask-HQ. Although the activation is inhibited globally, the feature patterns after LI layer are generally easier to recognise mainly due to the clarifications on semantic contours.

LI-Convs. Besides, the segmentation predictions generated by our method have better visual qualities, which also verifies the superiority of the LI-Convs.

5 Conclusion

We describe a dilated convolution with lateral inhibitions (LI-Convs) to enhance the model’s sensitivity to semantic contours and to extract features at denser scales. The performance of the proposed LI-ASPP and LI-MNV2 architectures is shown to outperform the baseline method on three segmentation benchmark datasets, which verify the effectiveness and generality of the LI-Convs. We also investigate and try to understand the working mechanisms hidden behind. The proposed LI-Convs can be seamlessly integrated into deep models for other tasks, such as lip-reading and object detection, that require explicit awareness of the semantic boundaries.

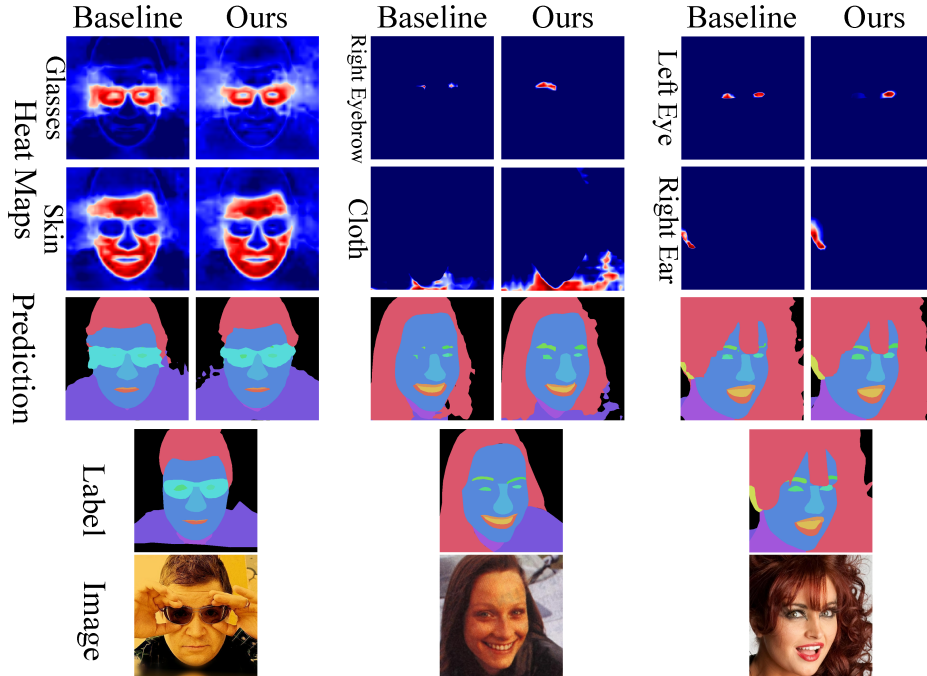


Figure 5: Visualisations of the class-level heat maps and semantic predictions of the baseline (MNV2+ASPP) and our method (LI-MNV2+LI-ASPP) on CelebAMask-HQ. Deeper reds in heat maps represent higher positive responses or more attention from the model, and vice versa for deeper blues. Our method allocates more attention to shape the semantic boundary areas and thus can produce predictions with higher visual qualities.

References

- [1] M. Abadi, A. Agarwal, P. Barham, E. Brevdo, Z. Chen, C. Citro, G. S. Corrado, A. Davis, J. Dean, M. Devin, et al. Tensorflow: Large-scale machine learning on heterogeneous distributed systems. *arXiv preprint arXiv:1603.04467*, 2016.
- [2] V. Badrinarayanan, A. Kendall, and R. Cipolla. Segnet: A deep convolutional encoder-decoder architecture for image segmentation. *IEEE transactions on pattern analysis and machine intelligence*, 39(12):2481–2495, 2017.
- [3] C. Cao, Y. Huang, Z. Wang, L. Wang, N. Xu, and T. Tan. Lateral inhibition-inspired convolutional neural network for visual attention and saliency detection. In *Thirty-Second AAAI Conference on Artificial Intelligence*, 2018.
- [4] S. Chandra and I. Kokkinos. Fast, exact and multi-scale inference for semantic image segmentation with deep gaussian crfs. In *European Conference on Computer Vision*, pages 402–418. Springer, 2016.
- [5] L.-C. Chen, M. Collins, Y. Zhu, G. Papandreou, B. Zoph, F. Schroff, H. Adam, and J. Shlens. Searching for efficient multi-scale architectures for dense image prediction. In *Advances in neural information processing systems*, pages 8699–8710, 2018.
- [6] L.-C. Chen, G. Papandreou, I. Kokkinos, K. Murphy, and A. L. Yuille. Semantic image segmentation with deep convolutional nets and fully connected crfs. *arXiv preprint arXiv:1412.7062*, 2014.
- [7] L.-C. Chen, G. Papandreou, I. Kokkinos, K. Murphy, and A. L. Yuille. Deeplab: Semantic image segmentation with deep convolutional nets, atrous convolution, and fully connected crfs. *IEEE transactions on pattern analysis and machine intelligence*, 40(4):834–848, 2018.
- [8] L.-C. Chen, G. Papandreou, F. Schroff, and H. Adam. Rethinking atrous convolution for semantic image segmentation. *arXiv preprint arXiv:1706.05587*, 2017.
- [9] L.-C. Chen, Y. Zhu, G. Papandreou, F. Schroff, and H. Adam. Encoder-decoder with atrous separable convolution for semantic image segmentation. In *ECCV*, 2018.
- [10] F. Chollet. Xception: Deep learning with depthwise separable convolutions. In *Proceedings of the IEEE conference on computer vision and pattern recognition*, pages 1251–1258, 2017.
- [11] J. Dai, H. Qi, Y. Xiong, Y. Li, G. Zhang, H. Hu, and Y. Wei. Deformable convolutional networks. In *Proceedings of the IEEE international conference on computer vision*, pages 764–773, 2017.
- [12] M. Everingham, S. A. Eslami, L. Van Gool, C. K. Williams, J. Winn, and A. Zisserman. The pascal visual object classes challenge: A retrospective. *International journal of computer vision*, 111(1):98–136, 2015.
- [13] B. J. T. Fernandes, G. D. Cavalcanti, and T. I. Ren. Lateral inhibition pyramidal neural network for image classification. *IEEE transactions on cybernetics*, 43(6):2082–2092, 2013.
- [14] A. Fernández-Caballero, M. T. López, J. Serrano-Cuerda, and J. C. Castillo. Color video segmentation by lateral inhibition in accumulative computation. *Signal, Image and Video Processing*, 8(6):1179–1188, 2014.
- [15] B. Hariharan, P. Arbeláez, L. Bourdev, S. Maji, and J. Malik. Semantic contours from inverse detectors. In *2011 International Conference on Computer Vision*, pages 991–998. IEEE, 2011.
- [16] B. Hariharan, P. Arbeláez, R. Girshick, and J. Malik. Hypercolumns for object segmentation and fine-grained localization. In *Proceedings of the IEEE conference on computer vision and pattern recognition*, pages 447–456, 2015.
- [17] H. K. Hartline, H. G. Wagner, and F. Ratliff. Inhibition in the eye of limulus. *The Journal of general physiology*, 39(5):651–673, 1956.
- [18] K. He, X. Zhang, S. Ren, and J. Sun. Deep residual learning for image recognition. In *Proceedings of the IEEE conference on computer vision and pattern recognition*, pages 770–778, 2016.
- [19] M. Holschneider, R. Kronland-Martinet, J. Morlet, and P. Tchamitchian. A real-time algorithm for signal analysis with the help of the wavelet transform. In *Wavelets*, pages 286–297. Springer, 1990.

- [20] Z. Huang, X. Wang, L. Huang, C. Huang, Y. Wei, and W. Liu. Ccnet: Criss-cross attention for semantic segmentation. In *Proceedings of the IEEE International Conference on Computer Vision*, pages 603–612, 2019.
- [21] S. Ioffe and C. Szegedy. Batch normalization: Accelerating deep network training by reducing internal covariate shift. *arXiv preprint arXiv:1502.03167*, 2015.
- [22] J. Kiefer, J. Wolfowitz, et al. Stochastic estimation of the maximum of a regression function. *The Annals of Mathematical Statistics*, 23(3):462–466, 1952.
- [23] C.-H. Lee, Z. Liu, L. Wu, and P. Luo. Maskgan: Towards diverse and interactive facial image manipulation. In *IEEE Conference on Computer Vision and Pattern Recognition (CVPR)*, 2020.
- [24] J. Li, Y. Wu, J. Zhao, L. Guan, C. Ye, and T. Yang. Pedestrian detection with dilated convolution, region proposal network and boosted decision trees. In *2017 International Joint Conference on Neural Networks (IJCNN)*, pages 4052–4057. IEEE, 2017.
- [25] T.-Y. Lin, M. Maire, S. Belongie, J. Hays, P. Perona, D. Ramanan, P. Dollár, and C. L. Zitnick. Microsoft coco: Common objects in context. In *European conference on computer vision*, pages 740–755. Springer, 2014.
- [26] C. Liu, L.-C. Chen, F. Schroff, H. Adam, W. Hua, A. L. Yuille, and L. Fei-Fei. Auto-deeplab: Hierarchical neural architecture search for semantic image segmentation. In *Proceedings of the IEEE Conference on Computer Vision and Pattern Recognition*, pages 82–92, 2019.
- [27] J. Long, E. Shelhamer, and T. Darrell. Fully convolutional networks for semantic segmentation. In *Proceedings of the IEEE Conference on Computer Vision and Pattern Recognition*, pages 3431–3440, 2015.
- [28] B. Luo, J. Shen, S. Cheng, Y. Wang, and M. Pantic. Shape constrained network for eye segmentation in the wild. In *The IEEE Winter Conference on Applications of Computer Vision*, pages 1952–1960, 2020.
- [29] Z.-H. Mao and S. G. Massaquoi. Dynamics of winner-take-all competition in recurrent neural networks with lateral inhibition. *IEEE transactions on neural networks*, 18(1):55–69, 2007.
- [30] B. Martinez, P. Ma, S. Petridis, and M. Pantic. Lipreading using temporal convolutional networks. In *ICASSP 2020-2020 IEEE International Conference on Acoustics, Speech and Signal Processing (ICASSP)*, pages 6319–6323. IEEE, 2020.
- [31] S. Minaee, Y. Boykov, F. Porikli, A. Plaza, N. Kehtarnavaz, and D. Terzopoulos. Image segmentation using deep learning: A survey. *arXiv preprint arXiv:2001.05566*, 2020.
- [32] T. N. Nguyen, X. T. Nguyen, H. Kim, and H.-J. Lee. A lightweight yolov2 object detector using a dilated convolution. In *2019 34th International Technical Conference on Circuits/Systems, Computers and Communications (ITC-CSCC)*, pages 1–2. IEEE, 2019.
- [33] H. Noh, S. Hong, and B. Han. Learning deconvolution network for semantic segmentation. In *Proceedings of the IEEE international conference on computer vision*, pages 1520–1528, 2015.
- [34] C. Peng, X. Zhang, G. Yu, G. Luo, and J. Sun. Large kernel matters—improve semantic segmentation by global convolutional network. In *Proceedings of the IEEE conference on computer vision and pattern recognition*, pages 4353–4361, 2017.
- [35] M. A. Rahman and Y. Wang. Optimizing intersection-over-union in deep neural networks for image segmentation. In *International symposium on visual computing*, pages 234–244. Springer, 2016.
- [36] G. Rizzolatti and R. Camarda. Inhibition of visual responses of single units in the cat visual area of the lateral suprasylvian gyrus (clare-bishop area) by the introduction of a second visual stimulus. *Brain Research*, 1975.
- [37] O. Ronneberger, P. Fischer, and T. Brox. U-net: Convolutional networks for biomedical image segmentation. In *International Conference on Medical image computing and computer-assisted intervention*, pages 234–241. Springer, 2015.
- [38] B. Roska, E. Nemeth, L. Orzo, and F. S. Werblin. Three levels of lateral inhibition: A space–time study of the retina of the tiger salamander. *Journal of Neuroscience*, 20(5):1941–1951, 2000.
- [39] O. Russakovsky, J. Deng, H. Su, J. Krause, S. Satheesh, S. Ma, Z. Huang, A. Karpathy, A. Khosla, M. Bernstein, et al. Imagenet large scale visual recognition challenge. *International journal of computer vision*, 115(3):211–252, 2015.

- [40] M. Sandler, A. Howard, M. Zhu, A. Zhmoginov, and L.-C. Chen. Mobilenetv2: Inverted residuals and linear bottlenecks. In *CVPR*, 2018.
- [41] F. Shen and G. Zeng. Gaussian dilated convolution for semantic image segmentation. In *Pacific Rim Conference on Multimedia*, pages 324–334. Springer, 2018.
- [42] K. Simonyan and A. Zisserman. Very deep convolutional networks for large-scale image recognition. *arXiv preprint arXiv:1409.1556*, 2014.
- [43] C. Sun, X. Chen, L. Huang, and T. Shou. Orientation bias of the extraclassical receptive field of the relay cells in the cat’s dorsal lateral geniculate nucleus. *Neuroscience*, 125(2):495–505, 2004.
- [44] D. Sun, X. Yang, M.-Y. Liu, and J. Kautz. Pwc-net: Cnns for optical flow using pyramid, warping, and cost volume. In *Proceedings of the IEEE Conference on Computer Vision and Pattern Recognition*, pages 8934–8943, 2018.
- [45] G. Von Békésy. *Sensory inhibition*. Princeton University Press, 2017.
- [46] P. Wang, P. Chen, Y. Yuan, D. Liu, Z. Huang, X. Hou, and G. Cottrell. Understanding convolution for semantic segmentation. In *2018 IEEE winter conference on applications of computer vision (WACV)*, pages 1451–1460. IEEE, 2018.
- [47] Y. Wang, B. Luo, J. Shen, and M. Pantic. Face mask extraction in video sequence. *International Journal of Computer Vision*, 127(6-7):625–641, 2019.
- [48] Y. Wang, J. Shen, M. Dong, Y. Wu, S. Cheng, and M. Pantic. Dynamic face video segmentation via reinforcement learning. *arXiv preprint arXiv:1907.01296*, 2019.
- [49] B. Xu, C. Lu, Y. Guo, and J. Wang. Discriminative multi-modality speech recognition. *arXiv preprint arXiv:2005.05592*, 2020.
- [50] S. Yan, X. Xu, D. Xu, S. Lin, and X. Li. Image classification with densely sampled image windows and generalized adaptive multiple kernel learning. *IEEE transactions on cybernetics*, 45(3):381–390, 2014.
- [51] M. Yang, K. Yu, C. Zhang, Z. Li, and K. Yang. Denseaspp for semantic segmentation in street scenes. In *Proceedings of the IEEE Conference on Computer Vision and Pattern Recognition*, pages 3684–3692, 2018.
- [52] F. Yu and V. Koltun. Multi-scale context aggregation by dilated convolutions. *arXiv preprint arXiv:1511.07122*, 2015.
- [53] F. Yu, V. Koltun, and T. Funkhouser. Dilated residual networks. In *Proceedings of the IEEE conference on computer vision and pattern recognition*, pages 472–480, 2017.
- [54] H. Zhang, K. Dana, J. Shi, Z. Zhang, X. Wang, A. Tyagi, and A. Agrawal. Context encoding for semantic segmentation. In *Proceedings of the IEEE conference on Computer Vision and Pattern Recognition*, pages 7151–7160, 2018.
- [55] H. Zhao, J. Shi, X. Qi, X. Wang, and J. Jia. Pyramid scene parsing network. In *Proceedings of the IEEE conference on computer vision and pattern recognition*, pages 2881–2890, 2017.
- [56] B. Zhou, H. Zhao, X. Puig, S. Fidler, A. Barriuso, and A. Torralba. Scene parsing through ade20k dataset. In *Proceedings of the IEEE conference on computer vision and pattern recognition*, pages 633–641, 2017.
- [57] Y. Zhu and S. Newsam. Learning optical flow via dilated networks and occlusion reasoning. In *2018 25th IEEE International Conference on Image Processing (ICIP)*, pages 3333–3337. IEEE, 2018.
- [58] B. Zoph and Q. V. Le. Neural architecture search with reinforcement learning. *arXiv preprint arXiv:1611.01578*, 2016.